Supplementary Information (SI) for EES Batteries.
This journal is © The Royal Society of Chemistry 2026

Supplementary information

Effect of Nanoparticle Surface Modification on Lithium-Ion Transport in Composite Polymer Electrolytes

Meghan Burns[1,2], Musawenkosi K. Ncube[3], Dan McElheny[2], Michael Counihan[1], Larry A. Curtiss[1] Anh T. Ngo [1,3], Jordi Cabana[1,2,4], Sanja Tepavcevic[1*]

[1]Materials Science Division, Argonne National Laboratory, Lemont, IL 60439, United States

[2]Department of Chemistry, University of Illinois at Chicago, Chicago, IL 60607, United States

[3]Department of Chemical Engineering, University of Illinois at Chicago, Chicago, IL 60608, United States

[4] Energy Storage Research Alliance, Argonne National Laboratory, Lemont, IL 60439, United States

Corresponding author: sanja@anl.gov

Table of contents:

Figure S1: Bulk (R_b) and interfacial (R_{int}) resistance values

Figure S2: Transference number average values across multiple methods

Figure S3: Chronoamperometry graphs used in transference number calculations

Figure S4: Silane-coupling agent bonding on the surface of LLZO

Figure S5: Additional Raman Spectra

Figure S6: Protonation at different positions of the LLZO surface

Figure S7: Two-step protonation and silanation mechanism

Figure S8: Solid-state Proton NMR

Figure S9: Critical Current Density PEIS measurements

Figure S10: Conductivity of neat PEO-LiTFSI and 20 wt% TEGDME

Figure S11: Ionic conductivity of all samples at 30°C

Figure S12: Ionic conductivity for cooling and reheating cycles

Figure S13: Evolution of PEIS spectra at 60°C during thermal conditioning

Figure S14: DRT graphs with standard deviation for each sample

Sample	Bulk Resistance (R_b) (Ω cm^2)	Interfacial Resistance (R_{int}) (Ω cm^2)
20 wt% TEGDME	9	73
Neat Al_2O_3	15	80
A-174@Al_2O_3	16	125
A-174@LLZO	13	51
APTES@LLZO	26	200

Figure S1: Bulk electrolyte resistance (R_b) values extracted from PEIS measurements of CPEs using Li symmetric cells. R_b was determined from the high-frequency intercept of the Nyquist plot, while R_{int} was obtained from the diameter of the semicircle (difference between the high and mid frequency intercepts on the real axis). The separation of R_b and R_{int} highlights the distinction between bulk ionic transport and interfacial contributions across different electrolyte compositions.

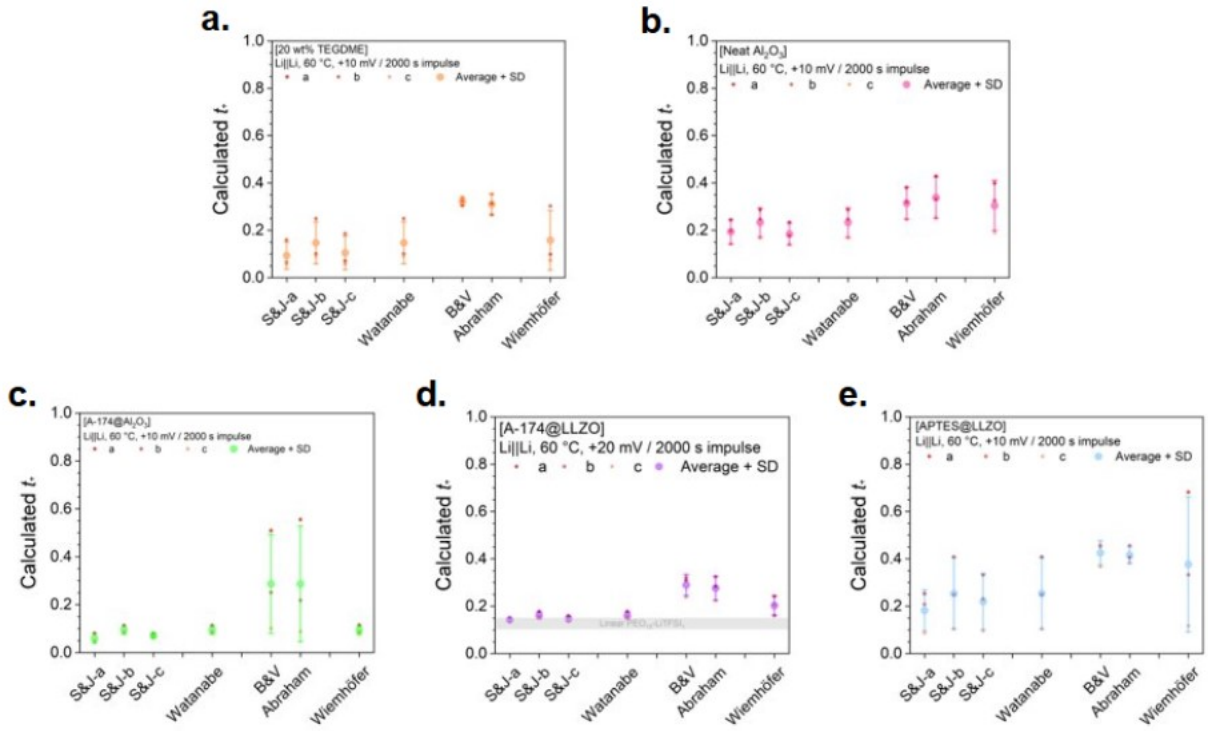

Figure S2: Transference number calculations for all seven known methods reported by Shaul Bublil et al. (*2022 J. Electrochem. Soc.* 169 110523): Sorenson and Jacobsen, Watanabe, Bruce and Vincent, Abraham, and Wiemhöfer. Each method was evaluated using three cells, with the average and standard deviation shown in each panel. All measurements were performed at 60°C with a + 10 mV applied bias and a 2000 s current pulse. Panel assignments correspond to the sample order in Figure S6: a) 20 wt% TEGDME, b) neat Al_2O_3, c) A-174@Al_2O_3, d) A-174@LLZO, and e) APTES@LLZO.

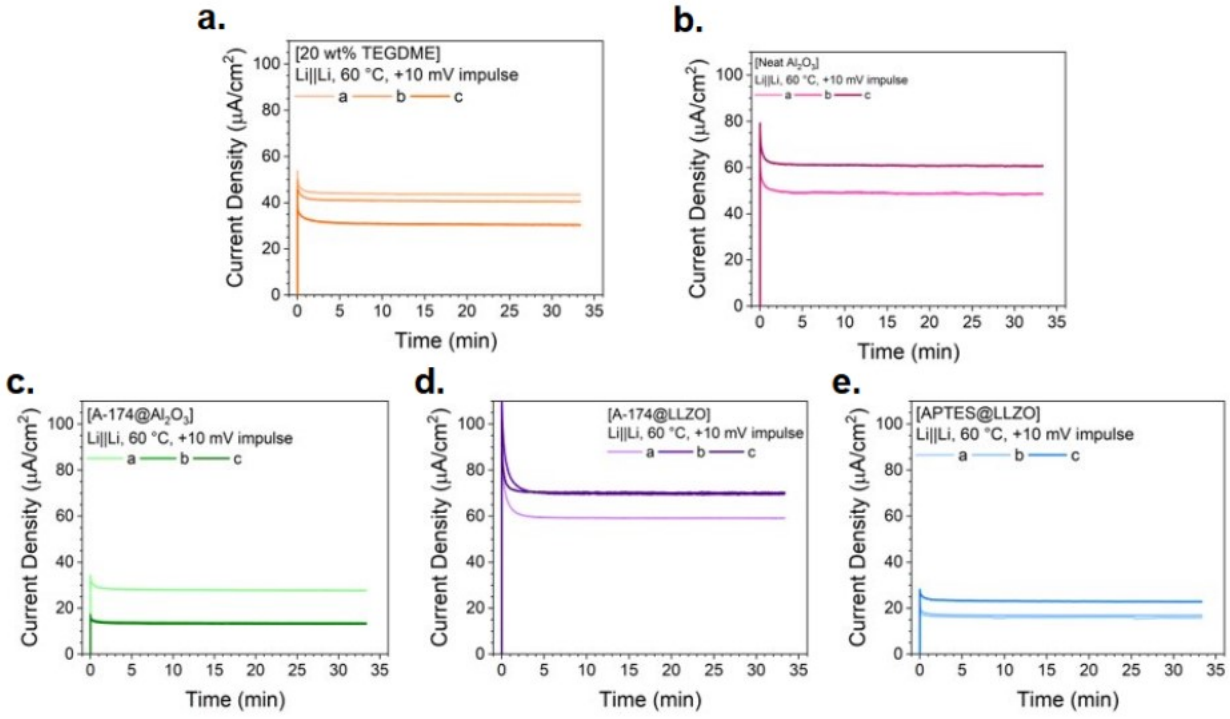

Figure S3: Chronoamperometry (CA) profiles from representative cells used in the transference number calculations. Three cells were measured for each sample corresponding to the data in Figure S7. All measurements were performed at 60°C with a + 50 mV applied bias, and the currents are normalized to the respective current densities. Panel assignments correspond to the sample order in Figure S6: a) 20 wt% TEGDME, b) neat Al_2O_3, c) A-174@Al_2O_3, d) A-174@LLZO, and e) APTES@LLZO.

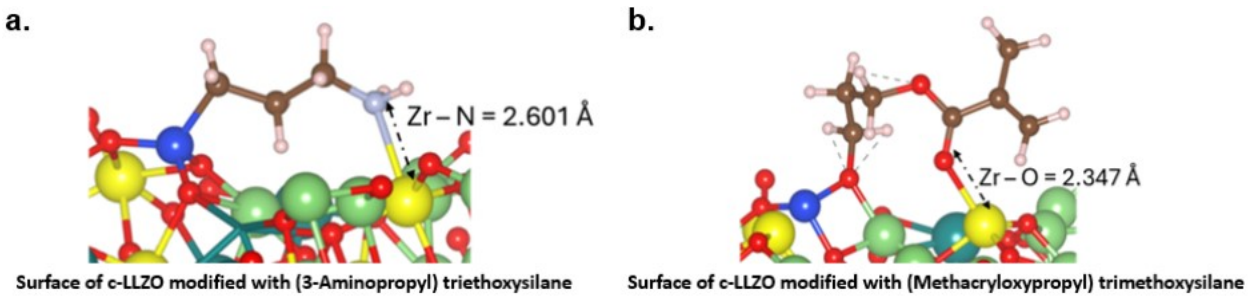

Figure S4: DFT-optimized interfacial geometries highlighting the bonding interactions between the two silane coupling agents used in this study and the LLZO surface. a) APTES bound to LLZO via a Zr-N bond with a calculated bond length of 2.601 Å. b) A-174 silane forming a Zr-O bond at the interface with a calculated bond length of 2.347 Å.

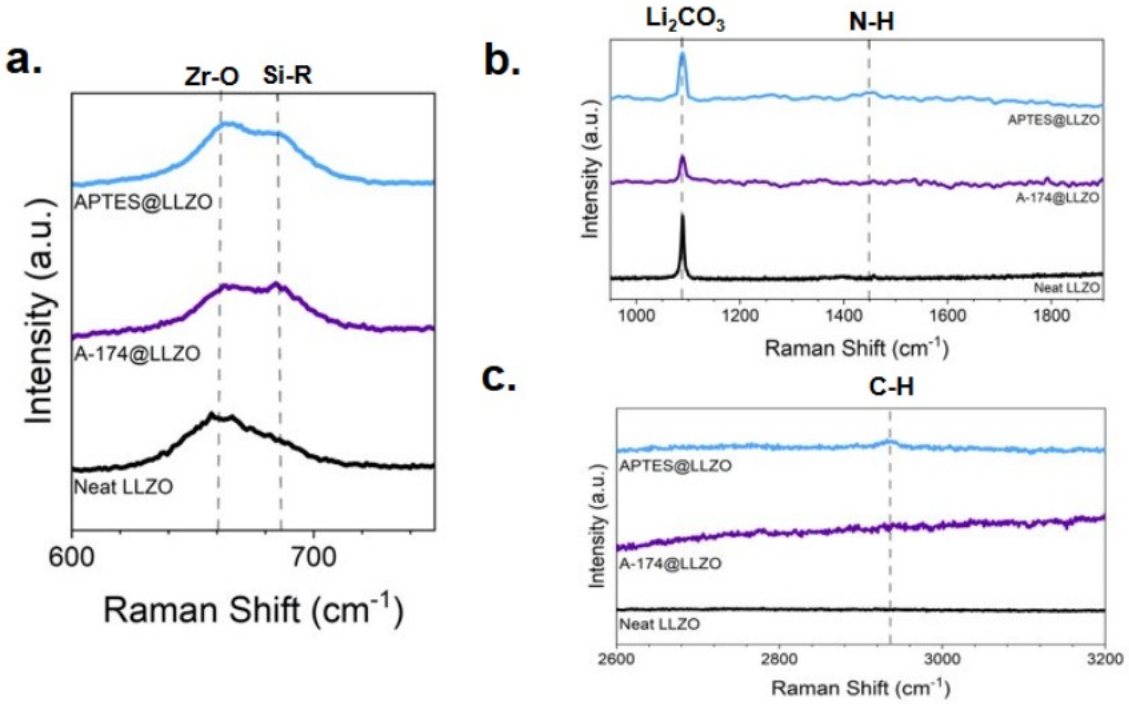

Figure S5: Additional Raman spectra collected across the full measurement range. a) Expanded view from 600-750 cm^{-1} highlighting the Zr-O and Si-R vibrational modes. b) Spectral region from 950-1850 cm^{-1} showing the N-H vibration associated with APTES. c) High-wavenumber region from 2600-3200 cm^{-1}, where a C-H stretching mode is observed only for the APTES-modified LLZO sample.

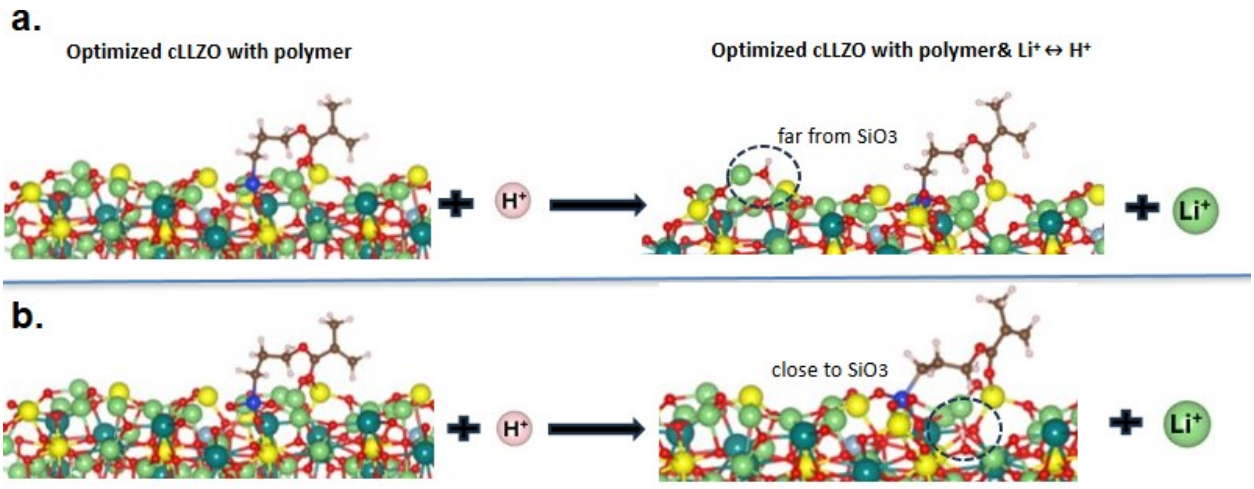

Figure S6: DFT optimized structures illustrating two possible protonation sites on the LLZO surface in the presence of silane A-174. a) Protonation at a site located farther away from the SiO_3 group. b) Protonation at a site adjacent to the SiO_3 group.

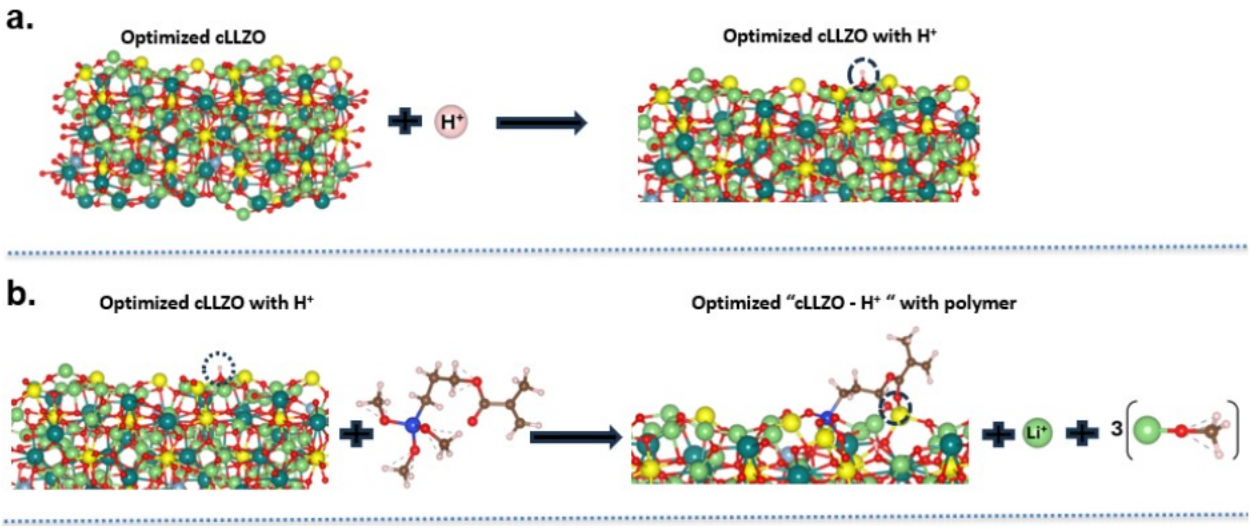

Figure S7: DFT-calculated geometries depicting the sequential protonation of LLZO and subsequent silane modification. a) Reaction of a proton binding to the bare LLZO nanoparticle. b) Protonated LLZO reacting with silane A-174, demonstrating formation of the LLZO-silane interface.

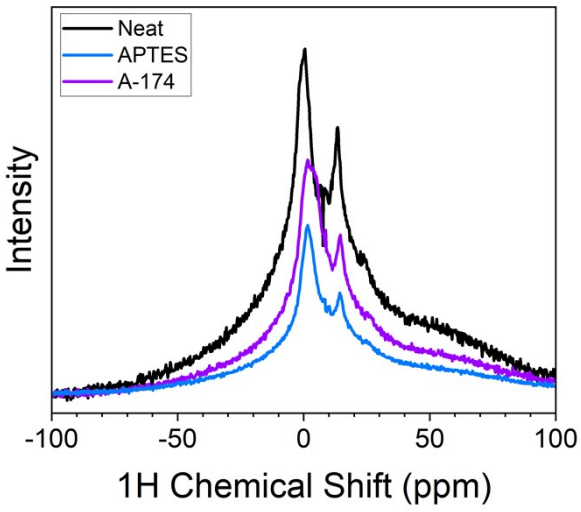

Figure S8: Proton solid-state NMR spectra of neat LLZO compared with APTES and A-174 modified LLZO, showing the effect of silane functionalization on proton environment.

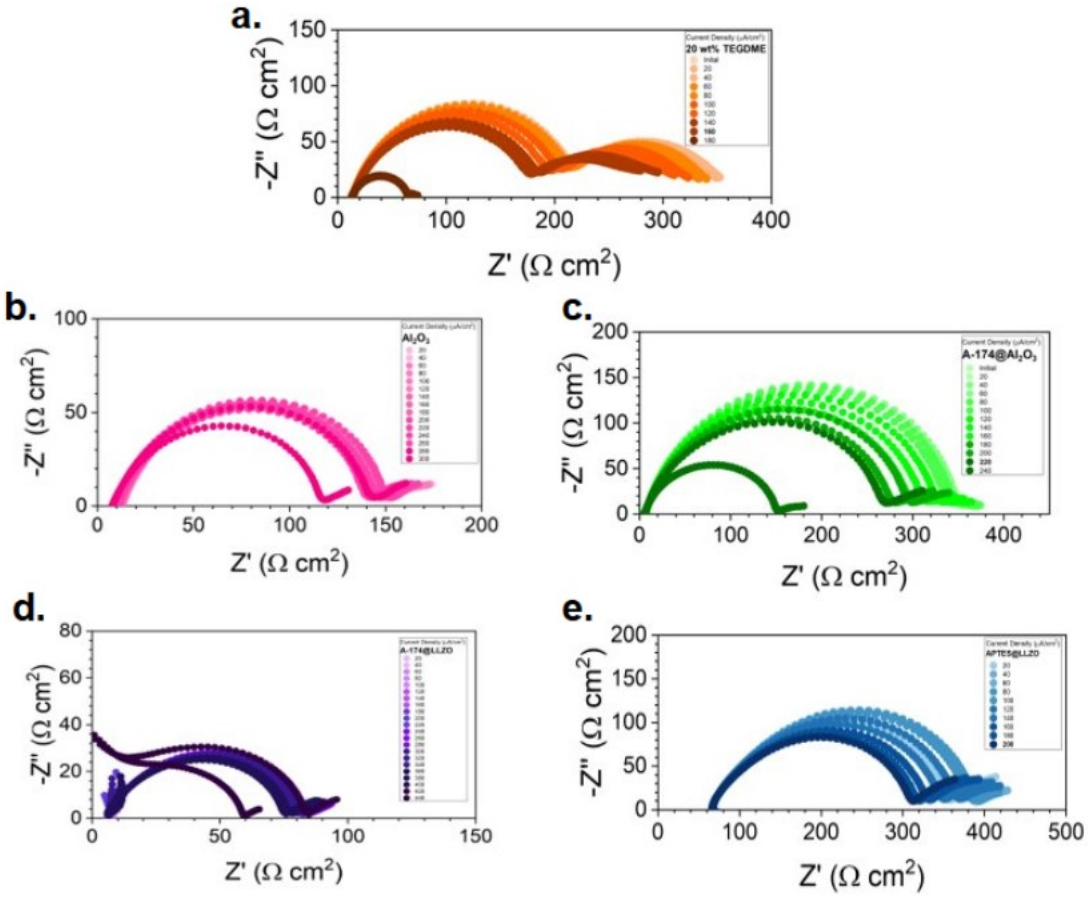

Figure S9: PEIS spectra measured after each current density step, corresponding to the critical current density galvanostatic cycling profiles shown in Figure 3 of the main text. a) 20 wt% TEGDME, b) neat Al_2O_3, c) A-174@Al_2O_3, d) A-174@LLZO, and e) APTES@LLZO.

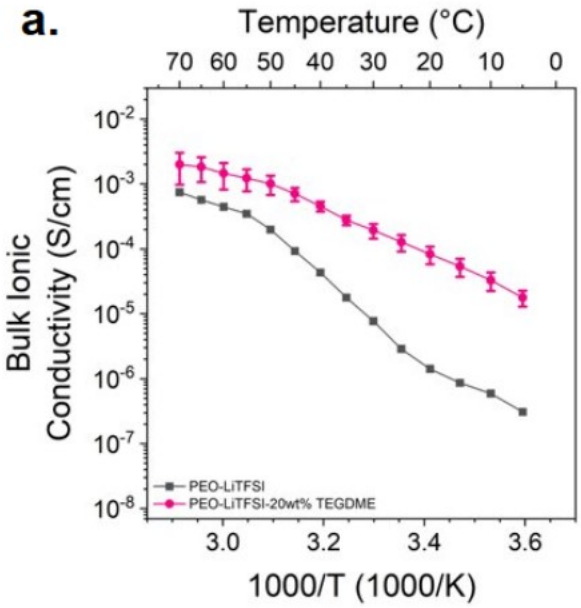

Figure S10: Bulk ionic conductivity of neat PEO-LiTFSI and PEO-LiTFSI- 20 wt% TEGDME, determined from Arrhenius analysis of PEIS measurements conducted from 5-70°C.

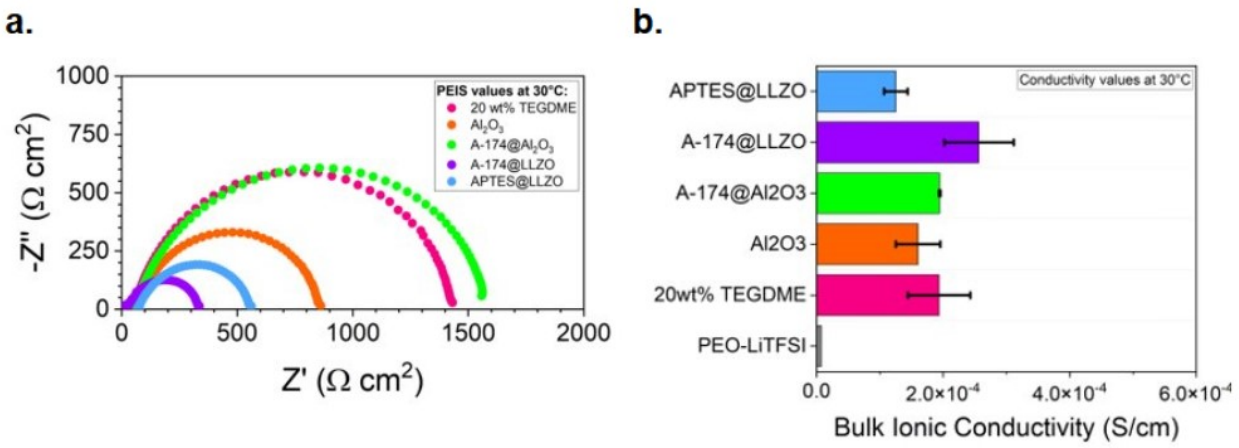

Figure S11: PEIS analysis of all samples at 30°C. a) Nyquist plots normalized to the electrode area. b) Corresponding bulk ionic conductivities with error bars at 30°C.

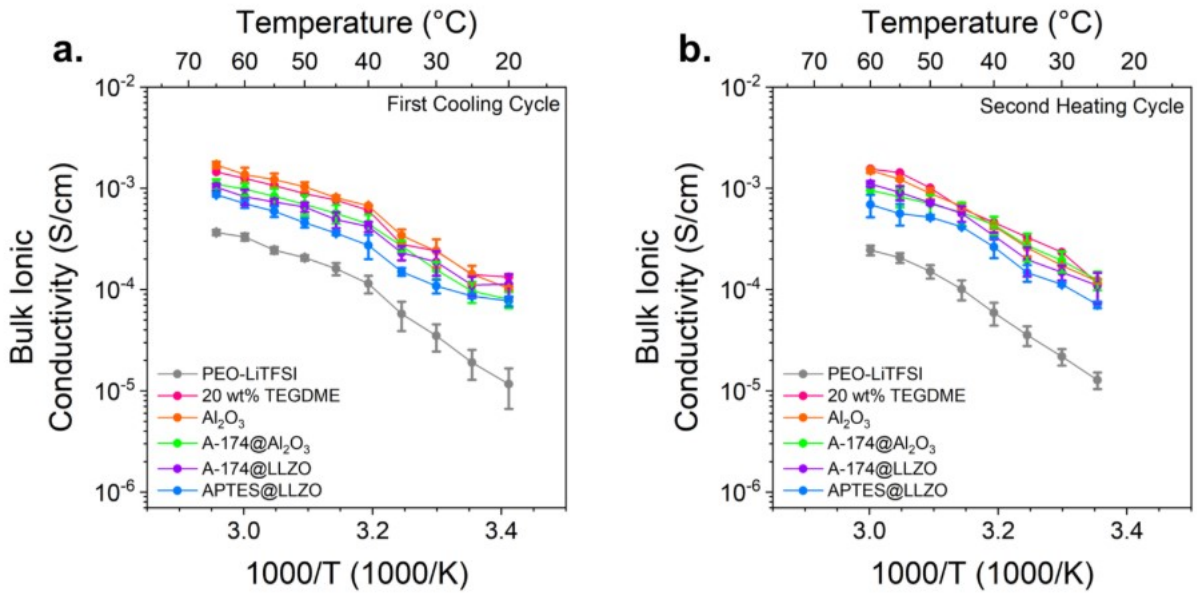

Figure S12: Arrhenius analysis of bulk ionic conductivity during thermal cycling. a) Cooling profile from 65°C to 20°C following the initial heating cycle. b) Reheating profile from 25°C to 60°C. These measurements were performed after the initial 5-70°C heating cycle, located in Figure 4a.

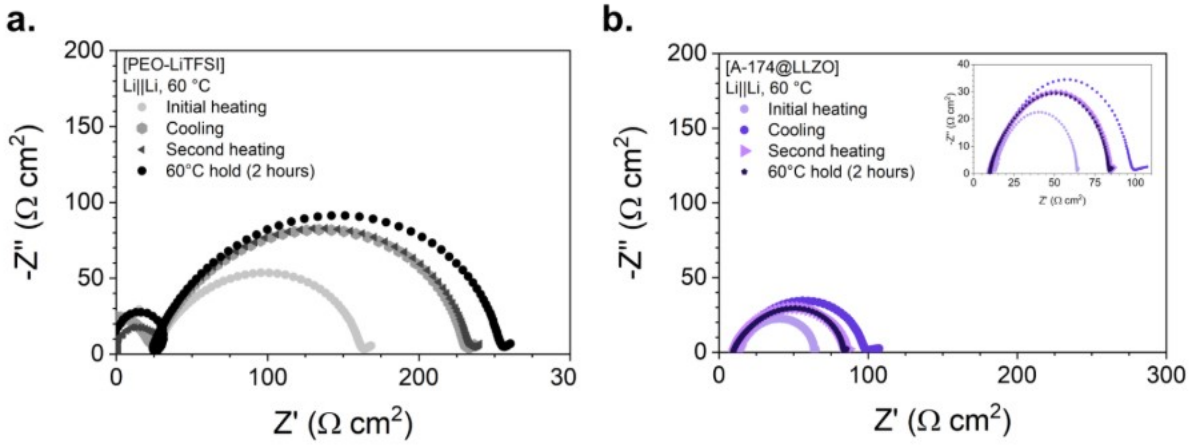

Figure S13: Potentiostatic electrochemical impedance spectroscopy (PEIS) spectra collected at 60°C at different stages of thermal cycling. a) Neat PEO-LiTFSI electrolyte. b) A-174@LLZO composite electrolyte. Spectra correspond to measurements taken at 60°C during the initial heating cycle, subsequent cooling cycle, second heating cycle, and after an isothermal hold at 60°C for 2 hours.

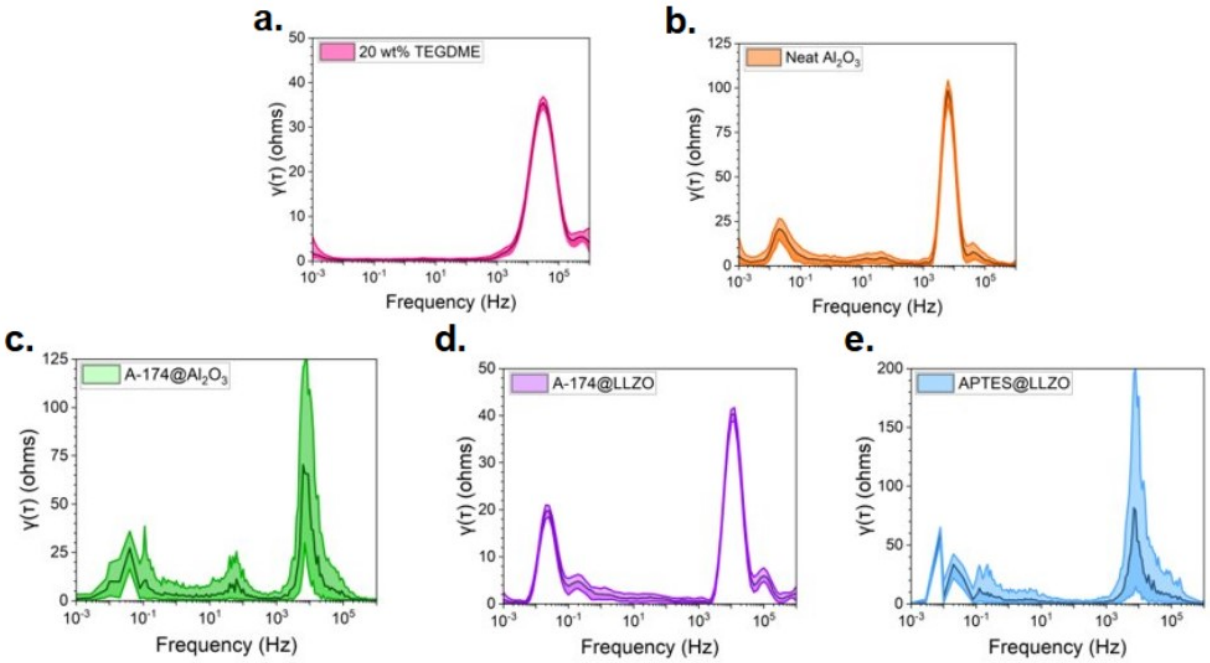

Figure S14: Distribution of relaxation times (DRT) for each sample. Uncertainty bands (shaded regions) were obtained via Monte Carlo resampling of the fitted PEIS spectra, with the shaded region corresponding to the standard deviation across 1000 realizations. All measurements were conducted at 60°C. Panel assignments correspond to the sample order in Figure S6: a) 20 wt% TEGDME, b) neat Al_2O_3, c) A-174@Al_2O_3, d) A-174@LLZO, and e) APTES@LLZO.